Materials Research Proceedings **15** (2020) 29-34 https://doi.org/10.21741/9781644900574-5

Wavelength-Resolved Neutron Imaging on IMAT

W. Kockelmann[1, a *], T. Minniti[1, b], R. Ramadhan[1,2, c], R. Ziesche[1,3 d], D.E. Pooley[1, e], S.C. Capelli[1, f], D. Glaser[4, g], A.S. Tremsin[5, h]

[1]STFC-Rutherford Appleton Laboratory, ISIS Facility, Harwell, OX11 0QX, UK

[2]University of Coventry, Centre Manufacturing and Materials Engineering, Coventry, CV1 5FB, UK

[3]University College London, Torrington Place, London, WC1E 7JE, UK

[4]Council for Scientific and Industrial Research (CSIR), Pretoria, South Africa

[5]University of California at Berkeley, Space Science Laboratory, CA 94720 Berkeley, USA

[a]winfried.kockelmann@stfc.ac.uk, [b]triestino.minniti@stfc.ac.uk, [c]ramadhar@uni.coventry.ac.uk, [d]ralf.ziesche.16@ucl.ac.uk, [e]daniel.pooley@stfc.ac.uk, [f]silvia.capelli@stfc.ac.uk, [g]dglaser@csir.co.za, [h]ast@ssl.berkeley.edu

* corresponding author

Keywords: Neutron Imaging, Neutron Radiography, Wavelength-Resolved Imaging, Energy-Selective, Energy-Dispersive, Time of Flight, Bragg Edge

Abstract. The IMAT project is now well into its commissioning phase, and a user programme for neutron imaging has started on the new instrument at ISIS TS2. The performance parameters for white-beam tomography and energy-dispersive neutron imaging had been determined earlier. Here we report on a further evaluation of the wavelength-resolving imaging options on IMAT, including selection of neutron wavelength bands using disk choppers as well as energy-dispersive Bragg edge imaging using time-resolving detectors. We review the instrument parameters of IMAT relevant for energy-resolved imaging, and present one example of residual strain imaging.

Introduction

Energy-selective and energy-dispersive neutron imaging has been developed over the past decade as discussed at many Neutron Wavelength Dependent Imaging (NeuWave) workshops [1] and as documented by many proof-of-concept and materials science studies [2], [3] (and references therein). Energy-selective neutron imaging using crystal monochromators was explored early on at continuous neutron sources [4, 5], whilst energy-dispersive Bragg edge transmission methods were developed on time of flight (TOF) instruments [6]. Further developments of energy-selective analysis at a pulsed neutron source [7] and the development of an MCP detector with high spatial and time resolution [8] helped to advance the field. Several dedicated TOF neutron imaging beamlines were designed in the past few years, with RADEN [9] and IMAT [3, 10] having started operation already.

Here we report on results from the commissioning of the IMAT instrument at the ISIS pulsed neutron source, UK. The basic performance parameters for white-beam tomography and energy-dispersive neutron imaging have been determined earlier [10], and a more application-related characterisation of the instrument was completed recently [11]. Here we continue to discuss the wavelength-resolving imaging options on IMAT, and report on the evaluation of energy-selection related instrument parameters.

Materials Research Proceedings **15** (2020) 29-34 https://doi.org/10.21741/9781644900574-5

IMAT set-up

IMAT is installed on the coupled 18 K liquid hydrogen (LH2) moderator of beam port W5 on the 10 Hz pulsed source TS2 of ISIS. Fig. 1 shows the main components; details of the instrument setup are given in [3] and [10]. The flight path length of the beamline from the moderator centre to the centre of the sample positioner is 56 m. Two double-disk choppers, a T_0 chopper, five vanadium-foil neutron monitors and different types of TOF detectors use an external trigger indicating at the time of the neutron pulse generation.

On IMAT there are three different detector systems available that take advantage of the TOF option. A gated light-intensified CCD camera can be used with the Messina camera box [3]. A microchannel plate detector (MCP) [8] uses a 2×2 array of Timepix readout chips (512×512 pixels, each 55×55 μm^2) and has a field of view of 28×28 mm^2. An active pixel sensor (GP2) uses the PImMS-2 CMOS and a gadolinium sheet for converting neutrons to electrons for a pixel size of 70×70 μm^2 and for a field of view of 22×22 mm^2 [12]. For each pixel of a TOF neutron camera (be it the gated-CCD, the MCP or the GP2) the time of the neutron arrival relative to the external trigger is measured, with an electronic time resolution of the order of 10 ns, i.e. well below the instrument resolution δλ.

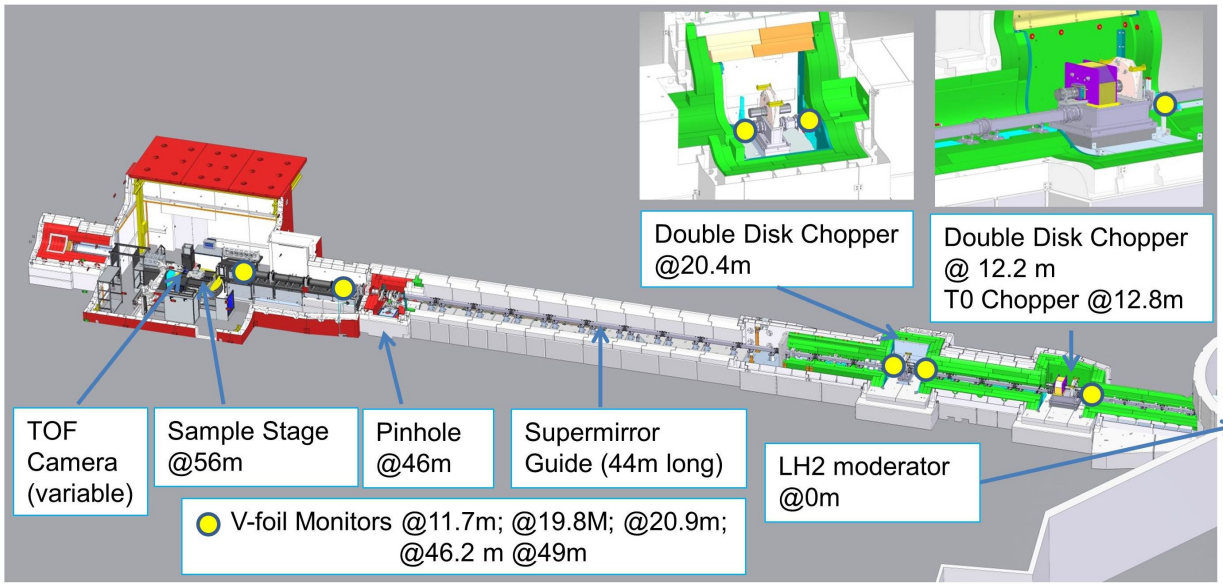

Fig. 1: Schematic overview of the IMAT instrument.

The wavelengths of the detected neutrons are calculated from their time of flight by

$$\lambda = \frac{h(T + \Delta T_0)}{mL} = 3957 * \frac{(T + \Delta T_0)}{L} \quad (1)$$

where λ is the neutron wavelength (in Angstrom), h is Planck's constant, T is the neutron time of flight (in seconds), ΔT_0 is the time offset of the source trigger received by the data processing electronics (in seconds), m is the neutron mass, and L is the flight path from source to detector (in meters). The maximum wavelength band, defined by the need to avoid frame overlap, is about 7 Å for L=56 m and 10 Hz operation [3]. The wavelength resolution of the instrument, on the other hand, is determined by the uncertainty δλ to which a given wavelength can be determined. The width and shape of the neutron pulse for a given wavelength depend on the type, geometry and physical (slowing down, storage) processes occurring within the moderator. The relative uncertainty δλ/λ, as determined recently for IMAT [10], defines the broadening of a Bragg edge or a Bragg dip in a TOF spectrum. It is this resolution function that signifies the

Materials Research Proceedings **15** (2020) 29-34 https://doi.org/10.21741/9781644900574-5

ability of the instrument to discriminate neutron energies, not the width of a time channel (in histogram mode) or uncertainty of a TOF measurement (in event mode).

Energy selection on IMAT

Energy-selective and energy-dispersive radiography enable image contrast enhancement and the mapping of structure properties, respectively. We use the terms energy-selective/dispersive synonymously with wavelength-selection/dispersion as the kinetic energy and the wavelength of a neutron follow from the measured time-of-flight via Eq 1. We use the term 'energy-selective' if one or more (wide or narrow) wavelength bands are engaged, with monochromatic neutron imaging being a special case. Energy-selection is a prerequisite for 'energy-dispersive' neutron imaging where histogramming within a wavelength range is performed with a sufficiently fine channel width that is smaller than the instrument resolution, for example by performing a scan across a Bragg edge.

The selection of neutron wavelength bands using the two double-disk choppers on IMAT is demonstrated in Fig. 2. The four disks running at 10 Hz can be 'phased' to select broader (Fig. 2a) or narrow (Fig. 2b) wavelength bands, up to the width of the white-beam spectrum (red curves). The narrow bands are defined by the condition not to reduce the peak flux (Fig. 2b), yielding relative band widths $\Delta\lambda/\lambda$ ranging from 30% to 10%, for wavelengths from 2 to 6.5 Å, respectively. For example, the bandwidth at the flux maximum of the IMAT spectrum at 2.6 Å is $\Delta\lambda/\lambda$~22% (blue curve in Fig 2b). Given these values, and that only one energy band is engaged at a time, this method allows energy-selective rather than energy-dispersive measurements.

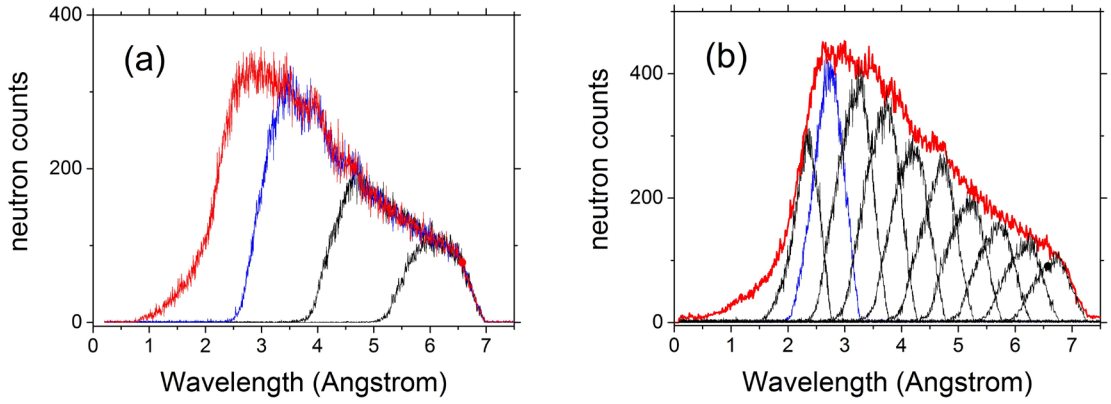

Fig, 2: Examples of wavelength band selection using choppers, for (a) broad and (b) narrow bands.

Coarse wavelength bandwidth selection is flexibly and quickly achieved via chopper dephasing from a script without changing beamline components. Experiments with a 'pink beam' (i.e. a narrow wavelength band; a term adopted from the synchrotron X-ray imaging community) allow for changing image contrasts without changing the sample set-up and for surveying energy-dependencies of attenuation coefficients for the largest field of view of IMAT (up to 20×20 cm^2) with any camera system. The neutron flux levels for the narrow wavelength bands in Fig. 2b are reduced to 3-7% of the white-beam flux (depending on wavelength) thus practically precluding tomography studies. Because of the coarse banding, detailed Bragg edge studies are not possible.

Another approach to achieve energy discrimination on a TOF instrument is to synchronise the imaging camera with the neutron source. An energy-selective radiography set-up with a gated image-intensified CCD or CMOS camera [7, 13] allows selecting a wide or narrow energy interval out of a white-beam spectrum. The energy discrimination is achieved for the maximum

Materials Research Proceedings **15** (2020) 29-34 https://doi.org/10.21741/9781644900574-5

possible field of view, and in principle for time bins smaller than the instrument resolution. Thus, Bragg edge studies can be performed in principle; however with the gated camera only one channel is selected at a time (different from a high frame-rate camera) and only a fraction of the neutron spectrum is used at a time. Therefore, mapping of Bragg edge parameters is usually not performed on IMAT with this camera system.

With the IMAT pixel detectors that accumulate counts into multiple time-slices (3100 for the MCP and 4096 for GP2) performance is improved tremendously, in terms of acquisition times, albeit for small field of views. For a TOF instrument it is important to determine the spectral resolution, i.e. the monochromacity for a given wavelength. An energy-dispersive radiography was collected from a cylindrical CaF_2 crystal of 20 mm thickness and 35 mm diameter, at a distance of 25mm from the MCP detector and with an L/D of 250 (Fig. 3a). Fig. 3b displays Bragg dips from the CaF_2 single crystal for a selected wavelength range. Fig. 3c shows the wavelength dependence of the FWHM as an indicator of the resolution function. An alternative description was given earlier [10] using the trailing tail (asymmetry τ) of Bragg edges from a CeO_2 powder, shown in Fig. 3c for comparison. The asymmetry τ, an indicator of the storage term of the moderator process and reflecting the peak broadening, is preferred to represent the resolution function of IMAT as it is sample-independent and can be determined with a calibration measurement. The FWHM values are smaller by about a factor of two; the scatter of the values is due to the FWHM dependence on wavelength and diffraction angle.

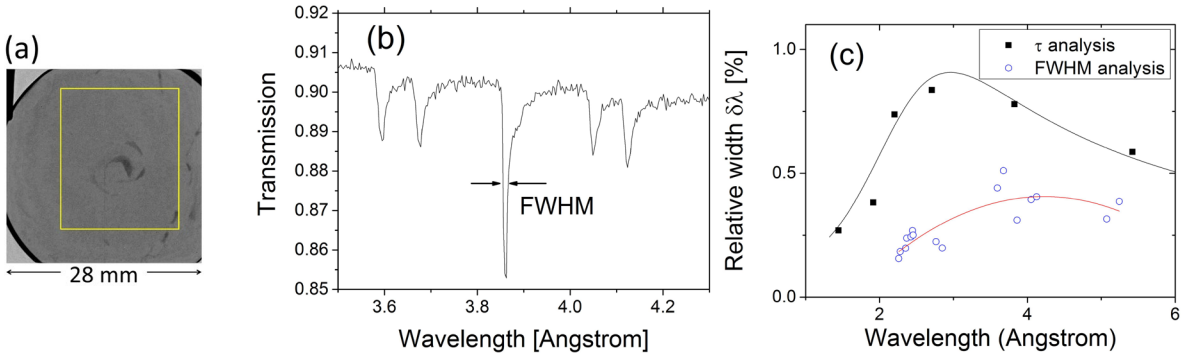

Fig. 3: (a) Radiography of a CaF_2 crystal; (b) Bragg dip spectrum for selected region of interest; (c) resolution function. "τ" data points taken from [10]. Solid curves are guides to the eye.

Table 1 summarises some of the instrument parameters of IMAT relevant for energy selective and energy-dispersive measurements for the different set-up options. The strain resolution value, demonstrating the precision with which a shift of a Bragg edge can be determined, is on the order of 0.01% for a good coherent scatterer like Fe, as determined earlier and included here for reasons of completeness [11]. The spatial resolution limit for Bragg edge analysis on IMAT is about 100 μm [11].

Strain mapping via Bragg edge analysis

A 12%Cr martensitic stainless steel sample with a laser-peened surface (see depiction in Fig. 4) relevant for steam turbine blade applications was analysed for two hours with an L/D of 125 using the MCP detector, with a time channel bin-width of 20 μs around the 110-Bragg edge. The distance of the face of the sample to the neutron-sensitive MCP was 20 mm. A transmission spectrum for a macro-pixel of 1.1 mm is shown in Fig 4. The 110-Bragg edge was fitted analytically using a Bragg edge profile (see [14] for details) based on the 'Santisteban' formula [6]. A strain map was reconstructed with a λ_0 value from the sample centre, far from the peened surface. A distinct zone of compressive residual strains ε_x is observed on the peened surface,

with a depth up to 1.5 mm, and a maximum compressive residual strain of about 1800 με on the surface. The typical strain error is ± 160 με. It should be noted that the analysed strain is averaged through the thickness of the sample along the beam direction.

Table 1: Energy-related instrument parameters of IMAT. See text for details.

White beam analysis: Single-frame bandwidth	 ~6 Å	Red curves in Fig. 2
Energy selection and 'pink beam' analysis using choppers: Energy resolution $\Delta\lambda/\lambda$	 22% at 2.6 Å	Blue curve in Fig. 2b
Energy-selection or -dispersion using a gated CCD: Energy resolution $\delta\lambda/\lambda$	 <0.9%	[7][13] [10] + Fig. 3c
Energy-selection or -dispersion and Bragg edge analysis using TOF detectors: Energy resolution: Bragg edge width, via "τ" analysis: $\delta\lambda/\lambda$ Energy resolution: Bragg dip width, via "FWHM" analysis: $\delta\lambda/\lambda$ Strain resolution: $\Delta\varepsilon=\Delta(\lambda-\lambda_0)/\lambda$ Spatial resolution for Bragg edge mapping	 <0.9% <0.45% 90 με >100 μm	 [10] + Fig. 3c Fig. 3c [11] [11]

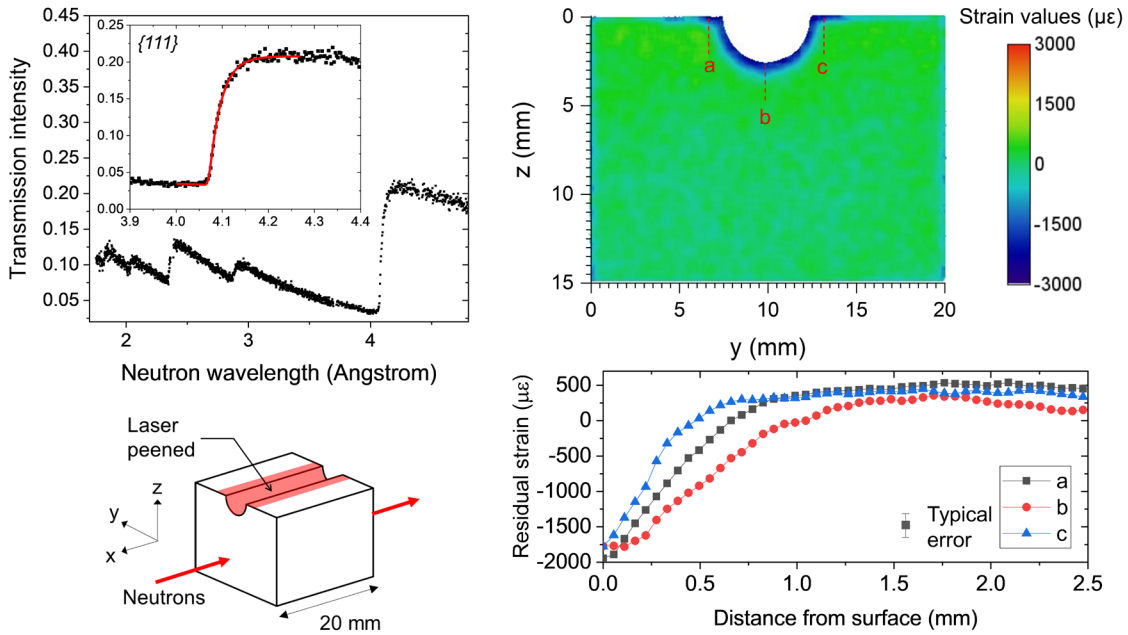

Fig. 4: Strain mapping of a laser-peened steel sample. (Top left) Bragg edge spectrum from a macro-pixel with analysed 110-Bragg edge in inset; (Top right) map of strain ε_x; (Bottom right) strain profiles for lines indicated in the strain map.

Conclusion

Coarse wavelength band selection using the IMAT disk choppers is aimed at enhancing contrasts of materials for large fields of views. For this mode, tomography scans are usually not considered because of the reduced neutron flux and low duty cycle. Much more important for the IMAT user programme are energy-dispersive measurements using the MCP or GP2 detectors given the unique possibilities for strain mapping on a TOF instrument. Other imaging methods that benefit from an energy-dispersive setup will be explored in due course, including wavelength-resolved interferometry, phase contrast imaging and grain mapping using attenuation, phase shift and/or diffractive signals.

References

[1] E.H. Lehmann, B. Schillinger, How the NEUWAVE workshop series has pushed neutron imaging developments, Neutron News 29 (2018) 25-31. https://doi.org/10.1080/10448632.2018.1445923

[2] R. Woracek, J.R. Santisteban, A. Fedrigo, M. Strobl, Diffraction in neutron imaging - a review, Nucl Instr Meth A 878 (2018) 141–158. https://doi.org/10.1016/j.nima.2017.07.040

[3] W. Kockelmann et al., Time-of-Flight neutron imaging on IMAT@ISIS: a new user facility for materials science**,** J. Imaging 4 (2018) 47. https://doi.org/10.3390/jimaging4030047

[4] N. Kardjilov, B. Schillinger, E. Steichele, Energy-selective neutron radiography and tomography at FRM, Applied Radiation and Isotopes 61 (2004) 455-460. https://doi.org/10.1016/j.apradiso.2004.03.070

[5] M. Schulz , P. Boni, E. Calzada, M. Muhlbauer, B. Schillinger, Energy-dependent neutron imaging with a double crystal monochromator at the ANTARES facility at FRM II, Nucl Instr Meth A 605 (2009) 33–35. https://doi.org/10.1016/j.nima.2009.01.123

[6] J.R. Santisteban, L. Edwards, A. Steuwer, P.J. Withers, Time-of-flight neutron transmission diffraction, J. Appl. Crystallogr. 34 (2001) 289–297. https://doi.org/10.1107/S0021889801003260

[7] W. Kockelmann, G. Frei, E. H. Lehmann, P. Vontobel, J. R. Santisteban, Energy-selective neutron transmission imaging at a pulsed source, Nucl Instr Meth A 578 (2007) 421-434. https://doi.org/10.1016/j.nima.2007.05.207

[8] A.S. Tremsin, J.V. Vallerga, J.B. McPhate, O.H.W. Siegmund, R. Raffanti, High resolution photon counting with MCP-Timepix quad parallel readout operating at > 1 KHz frame rates. IEEE Trans. Nucl. Sci. 60 (2013) 578–585. https://doi.org/10.1109/TNS.2012.2223714

[9] Y. Matsumoto, M. Segawa, T. Kai, T. Shinohara, T. Nakatani, K. Oikawa, K. Hiroi, Y.H. Su, H. Hayashida, J. D. Parker, S.Y. Zhang, Y. Kiyanagi, Recent progress of radiography and tomography at the energy-resolved neutron imaging system RADEN, Physics Procedia 88 (2017) 162-166. https://doi.org/10.1016/j.phpro.2017.06.022

[10] T. Minniti, K. Watanabe, G. Burca, D. Pooley, W. Kockelmann, Characterization of the new neutron imaging and materials science facility IMAT, Nucl Instr Meth A888 (2018) 184-195. https://doi.org/10.1016/j.nima.2018.01.037

[11] R.S. Ramadhan, W. Kockelmann, T. Minniti, B. Chen, D. Parfitt, M.E. Fitzpatrick, A.S. Tremsin, Characterisation and application of Bragg edge transmission imaging for strain measurement and crystallographic analysis on the IMAT beamline, J. Appl. Cryst 52 (2019) 351-368. https://doi.org/10.1107/S1600576719001730

[12] D.E. Pooley, J.W.L. Lee, M. Brouard, J.J. John, W. Kockelmann, N.J. Rhodes, E.M. Schooneveld, I. Sedgwick, R. Turchetta, C. Vallance, Development of the GP2 Detector: Modification of the PImMS CMOS Sensor for Energy-Resolved Neutron Radiography, IEEE TNS, 64 (2017) 2970-2981. https://doi.org/10.1109/TNS.2017.2772040

[13] T.E. McDonald Jr., T.O. Brun, T.N. Claytor, E.H. Farnum, G.L. Greene, C. Morris, Time-gated energy-selected cold neutron radiography, Nucl Instr Meth A 424 (1999) 235-241. https://doi.org/10.1016/S0168-9002(98)01252-2

[14] A.S. Tremsin, T.Y. Yau, W. Kockelmann, Non-destructive examination of loads in regular and self-locking spiralock® threads through energy resolved neutron imaging, Strain (2016). https://doi.org/10.1111/str.12201